Removal of captopril pharmaceutical from synthetic pharmaceutical-industry wastewaters: use of activated carbon derived from *Butia catarinensis*

Mariene R. Cunha[1], Eder C. Lima[1,2,3], Diana R. Lima[1], Raphaelle S. da Silva[1], Pascal S. Thue[3], Moaaz K. Seliem[4], Farooq Sher[5], Glaydson S. dos Reis[6], Sylvia H Larsson[6].

[1-]Postgraduate program in Mine, Metallurgical, and Materials Engineering (PPGE3M). School of Engineering, Federal University of Rio Grande do Sul (UFRGS), Av. Bento Gonçalves 9500, Porto Alegre, RS, Brazil

[2-] Institute of Chemistry, Federal University of Rio Grande do Sul (UFRGS), Av. Bento Goncalves 9500, Porto Alegre, RS, Postal Box, 15003, ZIP 91501-970, Brazil

[3-]Postgraduate program in Science of Materials (PGCIMAT). Institute of Chemistry, Federal University of Rio Grande do Sul (UFRGS), Av. Bento Gonçalves 9500, Porto Alegre, RS, ZIP 91501-970, Brazil

[4-] Faculty of Earth Science, Beni-Suef University, 62511, Egypt

[5-] School of Mechanical, Aerospace and Automotive Engineering, Faculty of Engineering, Environment and Computing, Coventry University, Coventry CV1 5FB, UK

6- Swedish University of Agricultural Sciences, Department of Forest Biomaterials and Technology, Biomass Technology Centre, SE-901 83 Umeå, Sweden

Abstract

A high surface area activated carbon was produced from the seed of *Butia catarinensis* (Bc), which was utilized for removing captopril from synthetic pharmaceutical industry wastewaters. The activated carbon was made by mixing $ZnCl_2$ and Bc at a proportion of 1:1 and pyrolyzed at 600° (ABc-600). The material was characterized by the Boehm titration, hydrophilic/ hydrophobic ratio, elemental analysis, TGA, FTIR, and N_2 isotherm (surface area (S_{BET}), total pore volume (TPV), and pore size distribution (PSD)). The characterization data showed that the adsorbent displayed a hydrophilic surface due to the presence of several polar groups. The carbon material presented a TPV of 0.392 $cm^3\,g^{-1}$, and S_{BET} of 1267 $m^2\,g^{-1}$. The equilibrium and kinetics data were suitably fitted to Liu isotherm and Avrami-fractional-order. The employment of the ABc-600 in the

treatment of synthetic pharmaceutical industry wastewater exhibited high effectiveness in their removals (up to 99.0%).

Keywords: Biomass adsorbent; activated carbon; emerging contaminant; efficient adsorption; mechanism of adsorption.

1. Introduction

Pharmaceuticals are used to improve the quality of life of humankind and domestic animals by curing diseases and prolonging longevity. However, the growing use of pharmaceutical products leads to releases of large amounts of drugs in pharmaceutical industry wastewaters (PIWW) [1], hospital effluents, and excretions of humans and livestock animals [2-5]. Ultimately, releases of drugs to waters are an environmental concern [2,3] because these compounds could affect living organisms and jeopardize the quality of the water resources [4].

Pharmaceuticals is one class of chemical compounds that are classified as emerging contaminants [3,6]. An emerging contaminant is a term used to describe synthetic or natural pollutants that have been detected in water bodies, which are not regularly monitored, which may cause ecological or human health impacts [3,6]. The pharmaceuticals in the environment come mainly from conventional wastewater treatment plants that are unable to remove these emerging concerns substances since they are not built to remove residual concentrations of these substances [5,7].

The treatment of waters and wastewaters containing pharmaceuticals is usually carried out using solar photo-Fenton [8,9], photolysis and photocatalysis [10-12], photo-Fenton electrochemical degradation [13], electrochemical oxidation [14], activated sludges [15,16], filtration [17,18], and adsorption [19-24]. However, these methodologies have shortcomings, such as high costs and high generation of sludges [25] and the formation of by-products [8,9]. This situation calls for further development of wastewater

63 treatment methods and, in particular, adsorption presents some advantages for the
64 treatment of effluents contaminated with pharmaceuticals, such as initial low cost for its
65 implementation and easy operation.

66 Captopril is an angiotensin-converting enzyme inhibitor (ACE) used for the treatment
67 of hypertension and some types of heart failure [26]. In Brazil, this medicine is given free-
68 of-charge for any Brazillian-resident with hypertension problem by the Brazillian Popular
69 Pharmacy Program [27]. Side effects of captopril have been reported as skin diseases
70 (*cutis laxa*) [28], and some health problems in newborns and young infants [26,28].
71 Besides these side effects, other problems can give rise with the prolonged use of
72 captopril (cough due to the increase in the plasma levels of bradykinin, taste alteration,
73 agranulocytosis, angioedema, hyperkalemia, proteinuria, teratogenicity, postural
74 hypotension, acute renal failure, and leukopenia [26,28]). Considering the expressive
75 consumption of captopril in Brazil, it is necessary to remove it from natural waters as well
76 as PIWWs.

77 Although captopril removal from aqueous wastewaters is essential from the health
78 and environmental viewpoint, there are few reports in the literature for the adsorption
79 treatment of this pharmaceutical [29-31]. Therefore, there is a need for the development
80 of new effective adsorbents for the removal of captopril from wastewaters.

81 The use of biochar and activated carbon for adsorption of pharmaceuticals is a hot
82 topic in the adsorption literature [3,24]. Low-cost biomass is pyrolyzed in the absence of
83 an oxygen atmosphere producing biochar. This carbon material can be utilized as is or
84 activated in ways that improve the textural properties, thereby presenting sorption
85 capacities similar to commercial activated carbons or other more expensive adsorbents
86 [3]. The carbon materials (biochar, activated carbons) presents aromatic rings with
87 several functional groups (carbonyl, carboxyl, phenol, esther), and other nitrogenated
88 aromatic groups (pyrrole, imidazole, and pyridinic) [23,24,32]. These functional groups
89 could interact with different organic compounds, such as pharmaceuticals products, by
90 Hydrogen bonding, π-π stacking, pair donor-acceptor of an electron, and van der Waals

interactions [23,24,33]. Besides, carbon adsorbent materials presenting high surface area, the high total volume of pores, and a suitable pore size distribution could contribute in a significant way for the removal of pharmaceuticals from aqueous effluents [23,24,30,32].

In this paper, the *Butia catarinensis* residues were used for activated carbon preparation. The *Butia catarinensis* belongs to the Arecaceae family, and it is easily found in the southern region of South America, mainly in the Brazilian states of Rio Grande do Sul and Santa Catarina [34]. Its fruits and leaves play an important socio-economic role in the region, where the leaves are utilized to fabricate hats, bags, and adornments [34]; the fruits are used for food production, and the seeds have no value and are usually discarded, motivating researches for employing such residue as a precursor for eco-friendly material production such activated carbon for water treatment.

Therefore, the seeds of the *Butia catarinensis* was utilized as a precursor for $ZnCl_2$-activated carbon preparation. The carbon material was characterized by isotherms of adsorption and desorption of nitrogen, FTIR, XRD, CHN/O elemental analysis, Bohem titration, hydrophobic/hydrophilic balance (HI), and pH_{pzc}. The kinetics, equilibrium, and thermodynamics of adsorption studies of captopril in the activated carbon were obtained, and the mechanisms of adsorption of captopril onto the carbon adsorbent were also proposed. After performing the characterization of the material and the batch-contact study of adsorption, the activated carbon was successfully employed for the removal of captopril from aqueous effluents and synthetic PIWW.

2. Material and methods

2.1 Materials

Deionized water was employed for preparing solutions. Captopril (CAS 62571-86-2; 217.283 g mol^{-1}; see Fig S1) was furnished by Sanofi-Medley (Campinas, Brazil). Zinc chloride, hydrochloric acid, sodium hydroxide (Neon, Brazil) of analytical grade were used as received.

2.2 Activated carbon

The preparation process of the activated carbon was as following: First, around 80.0 g of the shell of *Butia catarinensis* (Bc) was grounded (ϕ< 250 µm) and blended with 80.0 g of $ZnCl_2$ dissolved in 80 mL of water. These components were mechanically mixed to form a paste [35,36]. After drying it at 90°C for 2 h, the mixture was introduced in a quartz reactor in a ceramic oven. Then, the reactor was heated from 25° up to 600°C at 10 °C.min^{-1} under an N_2 flow rate of 150 mL.min^{-1}. The temperature of the furnace was kept fixed at 600°C for 30 minutes. Subsequently, the system was chilled under 150 mL min^{-1} of N_2 gas flow until the system attains < 200°C. To leach-out, the inorganics from the carbonized material, a 6M HCl solution was added to a known quantity of the obtained material under reflux (120 minutes) [35,36]. The carbon material after the leaching-out was denominated as ABc-600.

2.3 Characterization

Specific surface area (S_{BET}), pore-volume, and their distribution were obtained from N_2 Isotherm points as described in references [37,38].

The quantities of C, H, N, and O (%) were determined by carrying out the elemental analysis as described in [30,35,36,39].

An adapted Boehm-titration procedure was used to quantify the total amount of acidic and basic groups of the ABc-600 [40,41].

Fourier-transform infrared vibrational spectroscopy (FTIR) was employed to detect the main functional groups present on the surface of activated carbon qualitatively. The FTIR results were obtained by using a model 8300 Shimadzu spectrophotometer, using a resolution of 4 cm^{-1}, and 100 cumulative scans [42].

147 The thermal stability of the activated carbon was evaluated by thermogravimetric
148 analysis (TGA). The activated carbon was heated up from 20° to 1000°C, under a
149 synthetic air atmosphere [39]. The thermogravimetric curve of ABc-600 activated carbon
150 was obtained under a synthetic air atmosphere from room temperature up to 1000°C
151 using a rate of 10°C min^{-1} (Fig 2). This analysis aims to see the thermal stability of the
152 activated carbon under air, which is the atmosphere of work, and also obtain the contents
153 of ashes at 1000°C [37]. Although the standard method for obtaining the ashes contents
154 is carried out in a conventional porcelain crucible disposed in a muffle furnace at 600°C
155 under air, the error of this analysis is high because the burn of the organic biomass is
156 incomplete, and it could occur spattering of the sample in the muffle furnace. Therefore
157 the use of an oxidizing atmosphere is to obtain the content of the ash in the activated
158 carbon [39].
159 The hydrophilicity/hydrophobicity ratio (HI) was carried out as described elsewhere
160 [22,39,42].
161 The point of zero-charge (pH_{pzc}) of the prepared activated carbon was determined by
162 following the procedure described in reference [39].
163
164 *2.4 Experiments of batch adsorption*
165
166 The equilibrium experiments were performed employing the ABc-600 and captopril
167 as sorbing species [30,42]. Detailed information about the adsorption tests is shown in
168 the Supplementary Material.
169 The quantities of captopril in the solutions before and after adsorption experiments
170 were determined by UV spectroscopy [43-47].
171 Isotherm models were employed to analyze the fitness of the experimental data, and
172 their validation was executed by using the Bayesian Information Criterion (*BIC*), the
173 standard deviation of residues (*SD*), and $R^2_{adjusted}$ [48,49]. See more information in
174 Supplementary Material.

175

176 *2.5. Models of kinetics and isotherms of adsorption*

177

178 The kinetic adsorption data were evaluated by employing three models, such as
179 pseudo-first-order, pseudo-second-order, and Avrami fractional-order.

180 The equilibrium adsorption data were evaluated by employing isotherm models of
181 Langmuir [48], Freundlich [48], and Liu [48,50]. See further explanations in
182 Supplementary Material and references [42,48,50].

183

184 *2.6 Thermodynamics of adsorption*

185

186 To evaluate the influence of temperature as well as the interactions between the
187 activated carbon and Captopril, the thermodynamic process was studied by ranging
188 temperatures from 10 to 45°C [42,51,52]. See further explanations in Supplementary
189 Material.

190

191 *2.7. Synthetic effluent*

192

193 Two pharmaceutical-industry effluents containing seven medicines, two sugars,
194 three organics, one surfactant, and eight inorganic compounds were prepared, and their
195 compositions are shown in Table 1 [30,53,54]. The chemical composition of these
196 effluents is compatible with an industrial-pharmaceutical industry (the contents of the
197 seven pharmaceuticals). Also, the synthetic effluents are consistent with hospital
198 effluents (two sugars, three organics) being released in the hospital treatment
199 wastewater plant (one surfactant and several inorganics, usually present in hospital
200 sewers) [53,54].

201

202 The adsorption tests followed the same procedures described in the equilibrium

adsorption tests.

Insert Table 1

3. Results and discussion

3.1 Activated carbon *characterization.*

N_2 isotherm for ABc-600 activated carbon could be classified by IUPAC [37] type I(b) (see Fig 1), which is characteristic of microporous adsorbent (pores size diameter ranging from 1.0 – 3.5 nm). The PSD of ABc-600 presented the highest peak at 1.21 nm, then a second peak around 1.47 nm, a third broader peak 2.16-2.73 nm, and the fourth shoulder at 3.43 nm. After this last peak, the distribution of the pores decreases to approximately zero, which shows that ABc-600 activated carbon has, besides a portion of micropores, also a small portion of mesopores.

The N_2 adsorbed volume by ABc-600 was 433.4 cm^3g^{-1}, the S_{BET} was 1267 m^2g^{-1} and the TPV were 0.392 cm^3 g^{-1}. These values are in agreement with previous papers [23,30,32]. Lima et al. [23] prepared activated carbon from Brazil nutshell, using two proportions of biomass: $ZnCl_2$ (1:1, and 1:1.5). The surface area of these materials were 1457 and 1640 m^2g^{-1}, and TPV of 0.6661 and 0.9290 cm^3g^{-1} for biomass: $ZnCl_2$ of 1:1 and 1:1.5, respectively [23]. Kasperiski et al. [30] reported the preparation of activated carbons from *Caesalpinia ferrea* seed pod wastes. These authors prepared three activated carbons with different proportions of biomass: $ZnCl_2$ (1:0.5, 1:1, and 1:1.5), and they obtained surface areas of 1050, 1469, and 1480 m^2g^{-1}, and total pore volumes of 0.289, 0.401, and 0.572 cm^3g^{-1}, for activated carbons prepared in the proportion biomass: $ZnCl_2$ of 1:0.5, 1:1, and 1:1.5, respectively [30]. Leite et al. [32] prepared seven different activated carbons from avocado seed using a 2^2-factorial design with three central points. The values of surface area ranged from 1122-1587 m^2g^{-1}, TPV ranging from 0.600 to 0.0847 cm^3 g^{-1}. The difference of these activated carbons cited above is related to the chemical composition of the carbon source (percentage of

cellulose, hemicellulose, and lignin) present in each biomass, amount of $ZnCl_2$ utilized as an activating agent, temperature, and time of activation [32].

Insert Fig 1

Four different weight loss temperature ranges were observed in the TGA and DTA curves for the ABc-600 activated carbon (Fig 2). The first weight loss (3.41% of the total weight) took place within the temperature range from 28.6° to 74.1°C, corresponding to the loss of adsorbed H_2O. The second loss (1.56%) occurred in the interval of 74.1°-467.1°C, due to a water loss in the voids between AC particles and pores [23,39,42], thereby providing a measure for the thermal stability of the ABc-600 activated carbon. The third stage of weight loss was the most significant (92.40%). It was observed in a temperature range from 467.1° to 739.8°C. This stage is related to the carbon matrix decomposition in the activated carbon. The weight loss at the last stage, which took place in the presence of air at 739.8° to 1000°C, was only 0.36%. At this final temperature, the carbonaceous matrix was entirely oxidized [39], resting only the ashes contents of the ABc-600 activated carbon (2.17%). Therefore, the ashes content can be obtained by using a TGA analysis using an oxidizing atmosphere. The total weight loss of ABc-600 was 97.73% (Fig 2).

Insert Fig 2

FTIR was used to identify the presence of the functional groups on ABc-600 activated carbon (Fig 3). The band at 3402 cm^{-1} is assigned to stretching of O-H groups with intermolecular H bonding [35,55], and peaks at 2922 (asymmetric) and 2852 cm^{-1} (symmetric) are related to the C–H stretching [20,23,55]. The bands at 1566 cm^{-1} are attributed to the asymmetric stretching of O=C of carboxylates [55] and the small bands at 1462 and 1400 cm^{-1} to ring modes of aromatics [20,23,30]. The vibrational band at 1385 cm^{-1} identifies N-C bonds of amines or amides, or H-C [23,35,36]. At 1253 cm^{-1} can

be attributed to the C-O stretch of phenols or ethers [20,23,35]. The band at 1150 cm^{-1} is attributed to C-O of alcohols, and at 1120 cm^{-1} to the O-C-C stretch of an ester is identified [20,23,35]. The vibrational bands at 877 and 802 cm^{-1} might be assigned to out of plane C-H bends [20,23,35].

Insert Fig 3

The Boehm titration gives useful and quantitative information in terms of basic and acidic groups present on an adsorbent surface [40,41]. Total acidity of 0.5021 mmol g^{-1} and a basicity of 0.1144 mmol g^{-1} of the ABc-600 was obtained from the analysis. Hence, the number of acidic groups onto ABc-600 was 4.4 times higher than the total basic groups.

The C H N/O elemental composition of the ABc-600 was C: 72.56%, H: 1.99%, N: 1.83%, O: 21.35%. The ash content was 2.27%. The molar ratio of O/N was 10.21. Considering that oxygen functional groups onto ABc-600 could be due to phenols, carboxylic acids, linear esters, and ethers (see Fig 3) and that some oxygen groups are not acidic (linear esters and ethers), the results of total acidity and basicity is in agreement with the C H N/O elemental analysis.

The C H N/O analysis of the pristine *Butia catarinensis* (Bc) was C: 52.25%C, H: 6.42%, N: 1.01% N, and O: 39.82%. The ash content was 0.50%. When comparing the C H N/O analysis of pristine biomass and ABc-600 activated carbon, an increase of 38.87% in C and 81.19% in N, and a decrease of O by 86.51%, was obtained when activated carbon was formed. The hydrogen content was decreased by 3.23 times. The increase of C is expected [23,30,36] because volatile organic groups containing hydrogen and oxygen are released in the pyrolysis step. The increase in the percentage of nitrogen is due to the entrapment of it as pyrrole, imidazole, and pyridinic rings in activated carbon structure [23,42].

The hydrophobic/hydrophilic balance (HI) [22,39] of ABc-600 activated carbon was

0.819. This value is the ratio of sorption capacity of vapor of n-heptane by the sorption capacity of vapor of water, both adsorbed by the activated carbon, being the sorption capacities expressed in mg g^{-1} [22,39]. The sum of total acidity (0.5021 mmol g^{-1}) plus basicity (0.1144 mmol g^{-1}) was 0.6165 mmol g^{-1}. From the FT-IR analysis (Fig 3), the C H N/O elemental analysis, and the total number of functional groups present onto the ABc-600 activated carbon surface, it can be expected that the surface of this carbonaceous material would present some hydrophilicity, and this was confirmed by the HI balance [22,39].

The pH_{pzc} of ABc- activated carbon was 5.85 (Fig S2). The value obtained, which is also in agreement with the total number of acidic sites in ABc-600, which is higher than the basic groups on the activated carbon surface.

The XRD of the ABc- activated carbon is presented in Fig S3. A broad peak ranging from 2θ 15.8° to 32.0° and presenting a maximum at 2θ 24.65° corresponds to amorphous carbon. This figure shows that the treatment of the activated carbon with reflux of 6 M HCl is efficient for the removal of all zinc compounds formed during the pyrolysis, as earlier described [36].

3.2 Effect of pH and correlation with pK_a values of captopril

One of the first parameters that should be optimized for performing batch adsorption experiments is the effect of the initial pH on adsorbate removal. In Fig S4 exhibits the pH effect on the captopril removal by the ABc-600 activated carbon. At pH 2.5, the removal of captopril was 90.3%. It was increased up to 94.6% at pH 5.5, and from this pH up to 10.0, the percentage of removal was almost constant. For the next experimental adsorption works, the pH of captopril solutions was adjusted to 7.0, considering a neutralized solution being a suitable medium for effluent treatment.

According to the pH_{pzc} value of ABc-600 activated carbon (see Fig S2), at pH values < 5.85, the superficial charge of ABc-600 adsorbent is positive, and at pH values > 5.85,

the surface of ABc-600 activated carbon becomes negatively charged. Captopril presents two pK_a values (4.02 and 10.10, see Fig S1 and Fig S5). At 4.02 < pH < 10.10, the second species (B of Fig S5) is the predominant species. At pH 7.06, that is $\frac{(pKa1 + pKa2)}{2}$ 99.82% of captopril is presented as the species B. The specie B is negatively charged. Considering that at pH 7, both ABc-600 activated carbon and captopril are negatively charged, the mechanism of adsorption should not be an electrostatic attraction. This last mechanism is prevalent for dye adsorption [36]; however, for adsorption of pharmaceuticals, this is not the main mechanism of adsorption, as already reported [23,30,36,39,42].

3.3 Kinetics of adsorption.

The kinetics of adsorption of captopril for the ABc-600 activated carbon was studied at initial concentrations of the sorbing species of 450 and 900 mg L^{-1}. The parameters of the models and the kinetic curves are depicted in Table 2 and Fig. 4, respectively; BIC, SD, and R^2_{adj} values were utilized to analyze the fitting of the kinetic data as described in Supplementary Material. When R^2_{adj} value is nearer to 1.00 and also presents the lowest *SD* and BIC values, these statistical parameters can help to attain the choice of the best model that explains a physical phenomenon [42,48,49]. The data of Table 2 reveals that the Avrami model displayed R^2 values are nearer to 1.000, and also presented the lowest SD and BIC values. When $\Delta BIC \geq 10$, suggests that the model with lower BIC values is the most suitable [42,49] (see more explanation in Supplementary Material).

ΔBIC values among pseudo-first-order and Avrami were 67.53 and 71.20, and among pseudo-second-order and Avrami were 90.35-94.57. Therefore, Avrami-fractional is the model that best describes the kinetics of adsorption of captopril onto ABc-600 activated carbon.

Insert Fig 4

Insert Table 2

Considering that k_{Av} and k_2 have different units, and k_1 and k_{AV} present the same units, to compare the kinetic parameters, It was obtained the $t_{1/2}$ and $t_{0.95}$ [30,42] values (see Table 2), which is correlated to 50% and 95% of the adsorption sites saturation, respectively [30,42]. Taking into account that Avrami fractional-order was the most suitable model: the $t_{1/2}$ was 3.659-3.803 min, and the $t_{0.95}$ was 9.131-9.733 min. These results show that the kinetics of adsorption of captopril onto ABc-600 activated carbon is fast. Kasperiski et al. [30], using the general-order kinetic model, observed that values of $t_{0.5}$ and $t_{0.95}$ for adsorption of captopril onto activated carbon were 2.792-4.247 min and 22.11-40.30 min. Based on these values, it is possible to say that the kinetic process for captopril removal onto ABc-600 activated carbon is faster than onto activated carbon, previously prepared [30].

For the remaining adsorption experiments, the contact time was fixed at 30 min (which is much higher than $t_{0.95}$), to guarantee that such time is enough for the equilibrium to be reached [30,42].

The intraparticle diffusion plots of adsorption of captopril pharmaceutical onto ABc-600 adsorbent is presented in Fig S6. As seen in this figure, when q_t versus $\sqrt{t}$ was plotted; it was observed two linear sections. These results mean that the intraparticle is not the unique mechanism of adsorption [48]. The first linear stage corresponds to the intraparticle diffusion, and the second linear part corresponds to the diffusion of captopril into the smaller pores of ABc-600 adsorbent until the equilibrium establishment [48]. The k_{ip} was obtained from the slope of the first linear section. These values were 121.8 and 161.9 mg g^{-1} $min^{-0.5}$, for 450 and 900 mg L^{-1} of the adsorbate solution. Converting these units in mg g^{-1} h^{-1}, these values would be 943.5 and 1254 mg g^{-1} h^{-1}. Sompornpailin et al. [56] studying the adsorption of carbamazepine into MIL-53 adsorbent and it was obtained a k_{ip} of 13.86 mg g^{-1} $h^{-0.5}$. The same authors obtained k_{id} for ciprofloxacin using

several adsorbents, and they obtained k_{id} ranging from 9.82-14.62 mg g^{-1} $h^{-0.5}$ [56]. When these authors studied the adsorption of mefenamic acid in different adsorbents, the kid obtained ranged from 1.47 to 36.90 mg g^{-1} $h^{-0.5}$ [56]. Tran et al. [57] studying the adsorption of diclofenac in graphene oxide-based nanomaterials, 0.2202 to 2.1271 mg g^{-1} $min^{-0.5}$ [57]. The values of k_{id} obtained in this work for adsorption of captopril onto ABc-600 biochar are much higher than the values of k_{id} reported in the literature [56,57]. The high values of K_{id} showed in Fig S6, is compatible with an adsorbent with high porosity, which increases the intraparticle diffusion, and also corroborated by the results of the $t_{1/2}$ and $t_{0.95}$ reported in Table 2.

3.4 Equilibrium of adsorption

The isotherms adsorption for captopril onto ABc-600 activated carbon was performed, ranging temperature from 10° to 45°C (Table 3). The isotherm of adsorption of captopril onto ABc-600 activated carbon at 45°C is presented in Fig 5. The suitability of the isotherm models was tested and supported by BIC, SD, and R^2_{adj} values; the Liu isotherm gave the best fit: R^2_{adj} ranged from 0.9999 to 1.000, and the BIC and SD values attained the lowest values [42,49]. Concerning ΔBIC values (BIC Langmuir – BIC Liu, and BIC Freudlich – BIC Liu), all values were > 10. The ΔBIC of Langmuir and Liu ranged from 79.80 to 281.2, and the ΔBIC of Freundlich and Liu ranged from 94.23 to 251.1. Therefore, Liu was the most suitable model to describe the removal of captopril onto ABc-600 activated carbon.

Observing the most suitable model (Liu), at 45° C, the Q_{max} for ABc-600 activated carbon was 717.2 mg g^{-1} for captopril. At 25°C, Q_{max} was 556.7 mg g^{-1}. The K_g value increased with temperature (see Table 3), indicating that the process of adsorption of captopril onto ABc-600 activated carbon is endothermic.

Although the adsorption of several pharmaceuticals into different adsorbents is usual in the literature, for captopril, there are few reports [29-31]. Orona-Návar et al. [29], using

titanate nanotubes, obtained Q_{max} of 21.29 mg/g, according to the isotherm of Langmuir. Kasperiski and co-workers [30], using activated carbon produced from *Caesalpinia ferrea* seed pod wastes, obtained Q_{max} values of 280.7 (25°C) and 343.9 mg g^{-1} (45°C). Liu et al. [31] used a γ-Cyclodextrin metal-organic framework and obtained a percentage of removal of 12.59% of a solution 10 g L^{-1} in ethanol. However, these authors did not explore the isotherms of adsorption with captopril. Considering the values of Q_{max} reported in Table 3 for adsorption of captopril using ABc-600 activated carbon, it could be stated that this adsorbent has the potentiality for being applied for treating the pharmaceutical industry wastewaters with success, that will be presented below.

Insert Table 3

Insert Fig 5

3.5 Thermodynamic and mechanism adsorption

The values of changes in enthalpy (ΔH°) and entropy (ΔS°) of adsorption were calculated using the nonlinear Van't Hoff equation [58] since, according to Lima et al. [58], the linear Van't Hoff equation usually employed in the majority of the papers on thermodynamic of adsorption, lead to values of ΔH° and ΔS° lower when compared with the same values using a nonlinear approach (see Fig 6). The thermodynamic equilibrium constant [52] was obtained from the Liu isotherm model [52,58] for temperatures ranging from 293-318 K (10°-45°C) (Table 4). The changes in Gibb´s free energy (ΔG°) were < 0 for the temperature range chosen (Table 4), indicating that the adsorption process is spontaneous. The ΔH° was + 27.55 kJ.mol^{-1}. The magnitude of ΔH° matches with a physical adsorption process [59]. For 25 < ΔH° < 60 kJ/mol, the changes in enthalpy match with hydrogen bondings [59,60], which could indicate the physisorption process. When ΔH°< 20 kJ mol^{-1}, van der Waals interactions (ion-dipole, dipole-dipole, ion-induced dipole, dipole–induced dipole, and dispersion) govern the interactions among both activated carbon and captopril [59,60]. Also, this adsorption is defined as

424 physisorption [59,60].

425 Insert Table 4

426 Insert Fig 6

427 Taking into account the chemical and physicochemical structures of both captopril
428 and activated carbon (see Fig S1, S5, and Fig 7), the adsorption mechanisms can be
429 supposed to follow donor-acceptor interactions (n-π interaction) that occur among
430 aromatic rings in the activated carbon structure that act as an electron acceptor. The
431 carbonyl groups of captopril act as electron donors. Also, the O^- anion of the carboxylate
432 and the N of the proline group present at captopril act as electron acceptor [23,24].

433 Another meaningful interaction is the hydrogen bonding interactions of –OH of the
434 activated carbon with the nitrogen of the captopril structure, and COO^- of captopril that
435 corresponds to the predominant structure of captopril at pH 7 (see structure B of Fig S5)
436 [60].

437 The van der Waals interaction of C-C, also known as hydrophobic interactions, also
438 takes place [23,24].

439 Furthermore, considering the texture of the ABc-600 activated carbon, the pore-filling
440 mechanism, due to the high surface area of the material, should also exert one of the
441 most significant contributions to the adsorption of captopril pharmaceutical. In Fig 7, is
442 presented the diagrammatic scheme of a possible mechanism of adsorption of captopril
443 onto ABc-600 activated carbon.

444 Insert Fig 7.

445

446 *3.6. Synthetic pharmaceutical industry wastewater treatment.*

447

448 Considering the excellent characteristics of ABc-600 activated carbon for captopril
449 removal, it is supposed that the ABc-600 could be used for the treatment of wastewaters
450 of the pharmaceutical industry. Two synthetic pharmaceutical wastewaters (Table 1)
451 were employed for attaining the performance of activated carbon for the removal of

several pharmaceuticals mixed with some other organic and inorganic compounds usually found in wastewaters [42] (Fig 8).

The UV-Vis spectra of the two synthetic effluents were used to calculate the amount of chemicals removed (see Fig. 8). The spectrum scan was performed from 190 to 800 nm before and after the treatment of the effluent with the ABc-600 activated carbon. The amount of compounds removed (in percentage) was calculated according to area integration under the band of absorption, as earlier reported [23,30,42].

The results displayed high percentage removal of 99.0% for effluent A and 98.1% for effluent B. It is essential to highlight that ABc-600 activated carbon still presented high performance for the removal of organics, even when the concentration of the pollutants were doubled (see Table 1). These observations are an indication that ABc-600 activated carbon could be used for the treatment of real industry pharmaceutical wastewater.

4. Conclusion

The ABc-600 activated carbon was employed for the removal of captopril from aqueous effluents. From the data of characterization, the activation of the activated carbon with $ZnCl_2$ provoked a high porosity development in the activated carbon structure with an elevated BET surface area of 1267 m^2g^{-1}. The ABc-600 activated carbon also showed high thermal stability - up to 467.1°C under a synthetic air atmosphere.

The adsorption experimental equilibrium data was successfully fitted by the Liu isotherm model, reaching a Q_{max} of 717.2 mg g^{-1} for captopril at 45°C. The removal of captopril onto ABc-600 followed a spontaneous and endothermic process, and the ruling mechanism was donor-acceptor interactions (n-π interactions) between the aromatic rings of activated carbon with the carbonyl, O^- of carboxylate, and N of the proline groups of captopril, the hydrogen bonding, and the pore-filling of the activated carbon. The carbon material was also employed in the synthetic pharmaceutical wastewaters

480 treatment and displayed excellent outcomes, up to 99.0% of removal. These results
481 demonstrate the potential of using activated carbon from *Butia catarinensis* as an
482 effective adsorbent for real wastewater treatment.
483

484 **Funding**

485 The authors thank the Coordination of Improvement of Higher Education Personnel
486 (CAPES, Brazil), Foundation for Research Support of the State of Rio Grande do Sul
487 (FAPERGS), and National Council for Scientific and Technological Development (CNPq,
488 Brazil) for financial support. Also, G.S. dos Reis and S.H. Larsson thanks to the
489 Treesearch Postdoctoral program, Bio4Energy, a Strategic Research Environment
490 appointed by the Swedish government, and the Swedish University of Agricultural
491 Sciences.
492

493 **Acknowledgments**

494 The authors are grateful to the Nanoscience and Nanotechnology Center (CNANO-
495 UFRGS) of the Federal University of Rio Grande do Sul (UFRGS). We are also grateful
496 to ChemAxon for giving us an academic research license for the Marvin Sketch software,
497 Version 20.14.0 (http://www.chemaxon.com), 2020, used for molecule physical-chemical
498 properties.
499

References

[1] Ananya Shah, A., Shah, M., Characterisation, and bioremediation of wastewater: A review exploring bioremediation as a sustainable technique for pharmaceutical wastewater, Groundwater for Sustainable Development 11 (2020) 100383, Doi:10.1016/j.gsd.2020.100383.

[2] Sophia, C.A., Lima, E.C., Allaudeen, N., Rajan, S., Application of graphene-based materials for adsorption of pharmaceutical traces from water and wastewater- a review, Desalin. Water Treatm. 57 (2016) 27573–27586.

[3] Sophia, C.A., Lima, E.C., Removal of emerging contaminants from the environment by adsorption. Ecotoxicol. Environ. Saf. 150 (2018) 1–17.

[4] Bio, S, Nunes, B., Acute effects of diclofenac on zebrafish: Indications of oxidative effects and damages at environmentally realistic levels of exposure, Environ. Toxicol. Phar., 78 (2020),103394. Doi 10.1016/j.etap.2020.103394.

[5] Kümmerer, K., Pharmaceuticals in the Environment – A Brief Summary: Sources, fate, effect and risks, 3rd Edition, Springer-Verlag, Berlin, 2008, 521 p.

[6] NORMAN. The network of reference laboratories, research centres, and related organisations for monitoring of emerging environmental substances. www.norman-network.net. It was accessed on July 7th, 2020.

[7] Silva, B., Costa, F., Neves, I.C., Tavares, T. Psychiatric Pharmaceuticals as Emerging Contaminants in Wastewater. Springer, Heidelberg, 2015, 96 p.

[8] Della-Flora, A., Wilde, M. L., Thue, P.S, Lima, D.R., Lima, E.C., Sirtori, C. Combination of solar photo-Fenton and adsorption process for removal of the anticancer drug Flutamide and its transformation products from hospital wastewater. J. Hazard. Mater.,396 (2020), 122699. DOI:10.1016/j.jhazmat.2020.122699.

[9] Della-Flora, A., Wilde, M.l., Pinto, I.D.F., Lima, E.C., Sirtori, C., Degradation of the anticancer drug flutamide by solar photo-Fenton treatment at near-neutral pH: Identification of transformation products and in silico (Q)SAR risk assessment.

528 Environ. Res., 183 (2020) 109223. Doi:10.1016/j.envres.2020.109223.
529 [10] Lino e Freitas, J.R., Quintão, F.J.O., da Silva, J.C.C., Silva, S.Q., Aquino, S.F.,
530 Afonso, R.J.C.F., Characterisation of captopril photolysis and photocatalysis by-
531 products in water by direct infusion, electrospray ionisation, high-resolution mass
532 spectrometry and the assessment of their toxicities, International Journal of
533 Environmental Analytical Chemistry, 97 (2017) 42-55.
534 [11] Mahmoud, W.M.M., Kümmerer, K., Captopril, and its dimer captopril disulfide:
535 Photodegradation, aerobic biodegradation, and identification of transformation
536 products by HPLC–UV and LC–ion trap-MS^n. Chemosphere 88 (2012) 1170–1177.
537 [12] Kovacic, M., Papac, J., Kusic, H., Karamanis, P., Loncaric Bozic, A., Degradation
538 of polar and non-polar pharmaceutical pollutants in water by solar assisted
539 photocatalysis using hydrothermal TiO_2-SnS_2. Chem. Eng. J. 382, (2020), 122826.
540 Doi:10.1016/j.cej.2019.122826.
541 [13] Murrieta, M.F., Brillas, E., Nava, J.L., Sirés, I., Photo-assisted electrochemical
542 production of HClO and Fe^{2+} as Fenton-like reagents in chloride media for
543 sulfamethoxazole degradation, Sep. Purif. Technol, 250 (2020), 117236.
544 Doi:10.1016/j.seppur.2020.117236.
545 [14] dos Santos, A.J., Cabot, P.L., Brillas, E., Sires, I., A comprehensive study on the
546 advanced electrochemical oxidation of antihypertensive captopril in different cells
547 and aqueous matrices. Applied Catalysis B: Environmental 277 (2020) 119240.
548 Doi:10.1016/j.apcatb.2020.119240.
549 [15] Wang, G., Wang, D., Xu, Y., Li, Z., Huang, L., Study on optimisation and
550 performance of biological enhanced activated sludge process for pharmaceutical
551 wastewater treatment, Sci. Total Environ., 739 (2020), 140166, DOI
552 :10.1016/j.scitotenv.2020.140166.
553 [16] Gros, M., Ahrens, L., Levén, L., Koch, A., Dalahmeh, S., Ljung, E., Lundin, G.,
554 Jönsson, H., Eveborn, D., Wiberg, K., Pharmaceuticals in source-separated
555 sanitation systems: Fecal sludge and blackwater treatment, Sci. Total Environ. 703

(2020) 135530. Doi: 10.1016/j.scitotenv.2019.135530.

[17] Naddeo, V. Secondes, M.F.N., Borea, L., Hasan, S.W., Ballesteros, F. Jr., Belgiorno, V., Removal of contaminants of emerging concern from real wastewater by an innovative hybrid membrane process – Ultrasound, Adsorption, and Membrane ultrafiltration (USAMe®). Ultrason. Sonochem. 68 (2020), 105237. Doi:10.1016/j.ultsonch.2020.105237

[18] Ahsani, M., Hazrati, H., Javadi, M., Ulbricht, M., Yegani, R. Preparation of anti-biofouling nanocomposite PVDF/Ag-SiO2 membrane and long-term performance evaluation in the MBR system fed by real pharmaceutical wastewater. Sep. Purif. Technol. 249 (2020) 116938. Doi:10.1016/j.seppur.2020.116938.

[19] Jauris, I.M., Matos, C.F., Saucier, C., Lima, E.C., Zarbin, A.J.G., Fagan, S.B., Machado, F.M., Zanela, I., Adsorption of sodium diclofenac on graphene: a combined experimental and theoretical study, Phys. Chem. Chem. Phys., 19 (2016) 1526-1536.

[20] Saucier, C., Karthickeyan, P., Ranjithkumar, V., Lima, E.C., dos Reis, G.S., de Brum, I.A.S. Efficient removal of amoxicillin and paracetamol from aqueous solutions using magnetic-activated carbon, Environ. Sci. Pollut. Res., 24 (2017) 5918-5932.

[21] Wamba, A.G.N., Ndi, S.K., Lima, E.C, Kayem, J.G., Thue, P.S., Costa, T.M.H., Quevedo, A.B., Benvenutti, E.V., Machado, F.M., Preparation, characterisation of titanate nanosheet–pozzolan nanocomposite and its use as an adsorbent for removal of diclofenac from simulated hospital effluent, J. Taiwan Inst. Chem. Eng., 102 (2019) 321-329.

[22] dos Reis, G.S., Sampaio, C.H., Lima, E.C., Wilhelm, M., Preparation of novel adsorbents based on combinations of polysiloxanes and sewage sludge to remove pharmaceuticals from aqueous solutions, Colloids Surf. A, 497 (2016) 304–315.

[23] Lima, D.R., Hosseini-Bandegharaei, A., Thue, P.S., Lima, E.C., de Albuquerque, Y.R.T., dos Reis, G.S., Umpierres, C.S., Dias, S.L.P., Tran, H.N. Efficient

584 acetaminophen removal from water and hospital effluents treatment by activated
585 carbons derived from Brazil nutshells, Colloid Surf. A 583 (2019) 123966.
586 Doi:10.1016/j.colsurfa.2019.123966.
587 [24] Tran, H.N., Tomul, F., Nguyen, H.T.H., Nguyen, D.T., Lima, E.C., Le, G.T., Chang,
588 C.T., Masindi, V., Woo, S.H. Innovative spherical biochar for pharmaceutical
589 removal from water: Insight into adsorption mechanism, J. Hazard. Mater., 394
590 (2020) 122255. Doi:10.1016/j.jhazmat.2020.122255.
591 [25] Gopinath, K.P., Madhav, N.V., Krishnan, A., Malolan, R., Rangarajan, G. Present
592 applications of titanium dioxide for the photocatalytic removal of pollutants from
593 water: A review, Journal of Environmental Management 270 (2020) 110906. Doi:
594 10.1016/j.jenvman.2020.110906.
595 [26] Gantenbein, M.H., Bauersfeld, U., Baenziger, O., Frey, B, Neuhaus, T.,
596 Sennhauser, F., Bernet, V. Side effects of angiotensin converting enzyme inhibitor
597 (captopril) in newborns and young infants, J. Perinat. Med. 36 (2008) 448–452.
598 [27] Brazillian Popular Pharmacy Program. https://www.saude.gov.br/acoes-e-
599 programas/farmacia-popular. It was accessed on July 7th, 2020.
600 [28] Aquino, D.M., Maia, A.M.C.M., Villa, R.T., Villa, A.C.F.B.B., A rare side effect of
601 captopril: Acquired *cutis laxa*, Medicina Cutanea Ibero-Latino-Americana, 46
602 (2018), 42-45.
603 [29] Orona-Návar, C., García-Morales, R., Rubio-Govea, R., Mahlknecht, J.,
604 Hernandez-Aranda, R.I., Ramírez, J.G., Nigam, K.D.P., Ornelas-Soto, N.,
605 Adsorptive removal of emerging pollutants from groundwater by using modified
606 titanate nanotubes, J. Environ. Chem. Eng. 6 (2018) 5332‑5340.
607 [30] Kasperiski, F.M., Lima, E.C., Umpierres, C.S., dos Reis, G.S., Thue, P.S., Lima,
608 D.R. Dias, S.L.P., Saucier, C., da Costa, J.B., Production of porous activated
609 carbons from *Caesalpinia ferrea* seed pod wastes: Highly efficient removal of
610 Captopril from aqueous solutions. J. Clean. Prod., 197 (2018) 919-929.
611 [31] Liu, B., Li, H., Xu, X., Li, X., Lv, N., Singh, V., Stoddart, J.F., York, P., Xu, X., Gref,

612 R., Zhang, J. Optimised synthesis and crystalline stability of γ-cyclodextrin metal-
613 organic frameworks for drug adsorption. International Journal of Pharmaceutics,
614 514 (2016) 212-219.
615 [32] Leite, A.B., Saucier, C., Lima, E.C., dos Reis, G.S., Umpierres, C.S., Mello, B.L.,
616 Shirmardi, M., Dias, S.L.P., Sampaio, C.H., Activated carbons from avocado seed:
617 Optimization and application for removal several emerging organic compounds,
618 Environmental Science and Pollution Research, 25 (2018) 7647–7661.
619 [33] Clurman, A.M., Rodríguez-Narvaez, O.M., Jayarathne, A., de Silva, G.,
620 Ranasinghe, M.I., Goonetilleke, A., Bandala, E.R., Influence of surface
621 hydrophobicity/hydrophilicity of biochar on the removal of emerging contaminants,
622 Chemical Engineering Journal 402 (2020) 126277. Doi:10.1016/j.cej.2020.126277.
623 [34] P.N. Cruz, T.C.S. Pereira, C. Guindani, D.A. Oliveira, M.J. Rossi, S.R.S. Ferreira,
624 Antioxidant and antibacterial potential of Butia (*Butia catarinensis*) seed extracts
625 obtained by supercritical fluid extraction, J. of Supercritical Fluids 119 (2017) 229-
626 237.
627 [35] Puchana-Rosero, M.J., Adebayo, M.A., Lima, E.C., Machado, F.M., Thue, P.S.,
628 Vaghetti, J.C.P., Umpierres, C.S., Gutterres, M., Microwave-assisted activated
629 carbon obtained from the sludge of tannery-treatment effluent plant for removal of
630 leather dyes, Colloid Surf. A, 504 (2016) 105-115.
631 [36] Leite, A.J.B., Sophia A.C., Thue, P.S., dos Reis, G.S., Dias, S.L.P., Lima, E.C.,
632 Vaghetti, J.C.P., Pavan, F.A., de Alencar, W.S., Activated carbon from avocado
633 seeds for the removal of phenolic compounds from aqueous solutions, Desalin.
634 Water Treat., 71 (2017) 168-181.
635 [37] Thommes, M., Kaneko, K., Neimark, A.V., Olivier, J.P., Rodriguez-Reinoso, F.,
636 Rouquerol, J., Sing, K.S.W. Physisorption of gases, with special reference to the
637 evaluation of surface area and pore size distribution (IUPAC Technical Report).
638 Pure Appl. Chem. 87 (2015) 1051–1069.
639 [38] Jagiello, J., Thommes, M. Comparison of DFT characterisation methods based on

N_2, Ar, CO_2, and H_2 adsorption applied to carbons with various pore size distributions, Carbon, 42 (2004) 1227-1232.

[39] Umpierres, C.S., Thue, P.S., Lima, E.C., dos Reis, G.S., de Brum, I.A.S., de Alencar, W.S., Dias, S.L.P., Dotto, G.L., Microwave activated carbons from Tucumã (*Astrocaryum aculeatum*) seed for efficient removal of 2-nitrophenol from aqueous solutions, Environ. Technol., 39 (2018) 1173-1187.

[40] Goertzen, S.L., Theriault, K.D., Oickle A.M., Tarasuk, A.C., Andreas, H.A., Standardisation of the Boehm titration. Part I. CO_2 expulsion and endpoint determination. Carbon 48 (2010) 1252–1261.

[41] Oickle, A.M., Goertzen, S.L, Hopper, K.R, Abdalla, Y.O., Andreas, H.A., Standardisation of the Boehm titration: Part II. Method of agitation, the effect of filtering, and dilute titrant. Carbon 48 (2010) 3313-3322.

[42] Thue, P.S., Umpierres, C.S., Lima, E.C., Lima, D.R., Machado, F.M., dos Reis, G.S., da Silva, R.S., Pavan, F.A., Tran, H.N. Single-step pyrolysis for producing magnetic activated carbon from tucumã (*Astrocaryum aculeatum*) seed and nickel(II) chloride and zinc(II) chloride. Application for removal of Nicotinamide and Propanolol. J. Hazard. Mater., 398 (2020) 122903. Doi:10.1016/j.jhazmat.2020.122903.

[43] Lima, E.C., Barbosa Jr., F., Krug, F.J. Lead determination in biological material slurries by ETAAS using W-Rh permanent modifier. Fresenius J. Anal. Chem., 369 (2001) 496-501.

[44] Lima, E.C., Barbosa Jr., F., Krug, F.J., Tavares. A. Copper determination in biological materials by ETAAS using W-Rh permanent modifier. Talanta, 57 (2002)177-186.

[45] Lima, E.C., Brasil, J.L., Santos, A.H.D.P. Evaluation of Rh, Ir, Ru, W-Rh, W-Ir, and W-Ru as Permanent Modifiers for the Determination of Lead in Ashes, Coals, Sediments, Sludges, Soils, and Freshwaters by Electrothermal Atomic Absorption Spectrometry. Anal. Chim. Acta, 484 (2003) 233-242.

668 [46] Barbosa Jr., F., Lima, E.C., Krug, F.J. Determination of arsenic in sediment and soil
669 slurries by electrothermal atomic absorption spectrometry using W-Rh permanent
670 modifier. Analyst, 125 (2000) 2079-2083.
671 [47] Lima, E.C., Barbosa Jr., F., Krug, F.J., Guaita, U., Tungsten-Rhodium Permanent
672 Chemical Modifier for Lead Determination in Digests of Biological Materials and
673 Sediments by Electrothermal Atomic Absorption Spectrometry. J. Anal. At.
674 Spectrom. 14 (1999) 1601-1605.
675 [48] Lima, E.C., Adebayo, M.A., Machado, F.M. Chapter 3: Kinetic and Equilibrium
676 Models of Adsorption, in Carbon Nanomaterials as Adsorbents for Environmental
677 and Biological Applications, C.P. Bergmann, F.M. Machado, Eds. Springer
678 International Publishing, 2015 pp. 33–69.
679 [49] Schwarz, G.G.E., Estimating the dimension of a model. Ann. Stat. 6 (1978). 461–
680 464.
681 [50] Liu, Y., Xu, H, Tay, J.H., Errata, for “Derivation of a General Adsorption Isotherm
682 Model” by Y. Liu, H. Xu, and J. H. Tay. J. Environ. Eng. 132 (2006) 147-147.
683 [51] Lima, E.C., Hosseini-Bandegharaei, A., Moreno-Piraján, J.C., Anastopoulos, I., A
684 critical review of the estimation of the thermodynamic parameters on adsorption
685 equilibria. Wrong use of equilibrium constant in the Van’t Hoof equation for
686 calculation of thermodynamic parameters of adsorption, J. Mol. Liq., 273 (2019)
687 425-434.
688 [52] Lima, E.C. Hosseini-Bandegharaei, A, Anastopoulos, I. Response to “Some
689 remarks on a critical review of the estimation of the thermodynamic parameters on
690 adsorption equilibria. Wrong use of equilibrium constant in the van’t Hoff equation
691 for calculation of thermodynamic parameters of adsorption - Journal of Molecular
692 Liquids 273 (2019) 425–434”. Journal of Molecular Liquids, 280 (2019) 298-300.
693 [53] Caicedo, D.F., dos Reis, G.S., Lima, E.C., de Brum, I.A.S., Thue, P.S., Cazacliu,
694 B.G., Lima, D.R., dos Santos, A.H., Dotto, G.L. Efficient adsorbent based on
695 construction and demolition wastes functionalized with 3-

aminopropyltriethoxysilane (APTES) for the removal ciprofloxacin from hospital synthetic effluents. Journal of Environmental Chemical Engineering, 8 (2020), 103875. Doi:/10.1016/j.jece.2020.103875.

[54] M.B.Cristóvão, J.Torrejais, R.Janssens, P.Luis, B.Van der Bruggen, K.K.Dubey, M.K.Mandal, M.R.Bronze, J.G.Crespo, V.J.Pereira, Treatment of anticancer drugs in hospital and wastewater effluents using nanofiltration, Separation and Purification Technology 224 (2019) 273-280.

[55] Yadav, L.D.S., Organic Spectroscopy. Springer Science, Dordrecht, 2005. DOI 10.1007/978-1-4020-2575-4.

[56] Sompornpailin, D., Ratanatawanate, C., Sattayanon, C., Namuangruk, S., Punyapalaku, P. Selective adsorption mechanisms of pharmaceuticals on benzene-1,4-dicarboxylic acid-based MOFs: Effects of a flexible framework, adsorptive interactions and the DFT study, Science of The Total Environment 720 (2020) 137449. Doi:10.1016/j.scitotenv.2020.137449

[57] Tran, T.V., Nguyen, D.T.C., Le, H.T.N., Vo, D.V.N., Nanda, S., Nguyen, T.D. Optimization, equilibrium, adsorption behavior and role of surface functional groups on graphene oxide-based nanocomposite towards diclofenac drug, Journal of Environmental Sciences 93 (2020) 137-150.

[58] Lima, E.C., Gomes, A.A., Tran, H.N. Comparison of the nonlinear and linear forms of the van't Hoff equation for calculation f adsorption thermodynamic parameters ($\Delta S°$ and $\Delta H°$), J. Mol. Liq., 311 (2020) 113315. Doi:10.1016/j.molliq.2020.113315.

[59] Chang, R., Thoman-Jr, J.W. Chapter 17- Intermolecular forces, in Physical Chemistry for Chemical Sciences, University Science Books, 779-808, (2014).

[60] Lipkowski, P., Koll, A., Karpfen, A., Wolschann, P., An approach to estimate the energy of the intramolecular hydrogen bond, Chem. Phys. Lett. 10 (2002) 256-263.

List of Tables

Table 1. Synthetic wastewaters compositions.

Effluent Composition	**(mg L^{-1})**	
Pharmaceuticals	**Effluent A**	**Effluent B**
Captopril	50.0	100.0
Acetyl salicylic acid	10.0	20.0
Propranolol hydrochloride	10.0	20.0
Ciprofloxacin	10.0	20.0
Enalapril maleate	10.0	20.0
Paracetamol	10.0	20.0
Sodium diclofenac	10.0	20.0
Sugars		
Saccharose	25.0	50.0
Glucose	25.0	50.0
Organics		
Urea	10.0	20.0
Citric acid	10.0	20.0
Humic acid	10.0	20.0
Sodium dodecyl sulphate	5.0	10.0
Inorganics		
Ammonium phosphate	20.0	30.0
Ammonium chloride	20.0	30.0
Sodium sulphate	10.0	20.0
Sodium chloride	50.0	70.0
Sodium carbonate	10.0	20.0
Calcium nitrate	10.0	20.0
Magnesium chloride	10.0	20.0
Potassium nitrate	10.0	20.0
pH*	7.0	7.0

* final pH adjusted to 7.0

728

729 **Table 2**. Pseudo-first-order, pseudo-second-order, and Avrami-fractional order
730 parameters for adsorption of captopril onto ABc-600 activated carbon. Adsorbent dosage
731 of 1.5 g L^{-1}; initial pH of captopril 7.0; the temperature of 25°C.

	Initial concentration (mg L^{-1})	
	450.0	900.0
Avrami fractional-order		
q_e (mg g^{-1})	291.6	381.6
k_{AV} (min^{-1})	0.2078	0.2173
n_{AV}	1.558	1.601
$t_{1/2}$ (min)	3.803	3.659
$t_{0.95}$ (min)	9.733	9.131
R^2 adjusted	0.9996	0.9995
SD (mg g^{-1})	1.943	2.905
BIC	33.75	49.04
Pseudo-first-order		
q_e (mg g^{-1})	294.2	385.0
k_1 (min^{-1})	0.1864	0.1949
$t_{1/2}$ (min)	3.718	3.556
$t_{0.95}$ (min)	16.07	15.37
R^2_{adj}	0.9835	0.9820
SD (mg g^{-1})	13.26	18.01
BIC	105.0	116.6
Pseudo-second-order		
q_e(mg g^{-1})	309.8	404.8
k_2 (g mg^{-1} min^{-1})	$8.375.10^{-4}$	$6.765.10^{-4}$
$t_{1/2}$(min)	3.734	3.544
$t_{0.95}$ (min)	55.42	53.20
R^2_{adj}	0.9434	0.9400
SD (mg g^{-1})	24.54	32.83
BIC	128.3	139.4

732

733

734

735

736 **Table 3**. Parameters of the isotherm of Langmuir, Freundlich, and Liu models for the
737 adsorption of captopril onto ABc-600 activated carbon.

Langmuir	10°C	20°C	25°C	30°C	40°C	45°C
Q_{max} (mg g^{-1})	422.2	367.8	366.0	360.2	387.4	399.5
K_L (L mg^{-1})	0.09304	0.3930	1.824	1.759	40.47	7.413
R^2_{adj}	0.9948	0.9097	0.9029	0.9638	0.9872	0.9879
SD (mg g^{-1})	9.087	33.51	32.14	17.70	11.11	11.05
BIC	76.80	118.6	117.2	98.14	83.24	83.06
Freundlich						
K_F (mg g^{-1} (mg $L^{-1})^{-1/nF}$)	150.8	193.0	231.9	264.7	330.2	346.3
n_F	5.616	8.302	11.07	16.98	32.19	35.11
R^2_{adj}	0.9446	0.9862	0.9954	0.9994	0.9999	1.000
SD (mg g^{-1})	29.56	13.09	7.026	2.278	1.072	0.5972
BIC	114.6	88.48	68.57	32.53	8.409	-10.31
Liu						
Q_{max} (mg g^{-1})	444.2	513.1	556.7	586.4	692.6	717.2
K_g (L mg^{-1})	0.08555	0.1222	0.1463	0.1741	0.2481	0.2993
n_L	0.7811	0.2898	0.2174	0.1357	0.06409	0.06057
R^2_{adj}	1.000	0.9999	0.9999	1.000	0.9999	0.9999
SD (mg g^{-1})	0.7144	0.004873	0.02911	0.1141	0.004195	0.004017
BIC	-2.995	-162.6	-105.4	-61.70	-167.4	-168.8

738

739

740

741 **Table 4.** Thermodynamics of adsorption of captopril onto ABc-600 activated carbon.

T (K)	293	298	303	308	313	318
K_e	$1.859.10^4$	$2.655.10^4$	$3.178.10^4$	$3.783.10^4$	$5.391 .10^4$	$6.504.10^4$
ΔG° (kJ mol^{-1})	-23.13	-24.82	-25.68	-26.55	-28.35	-29.30
ΔS° (J $K^{-1}.mol^{-1}$)	-	178.7*	-	-	-	-
ΔH° (kJ mol^{-1})	-	27.55*	-	-	-	-

742 Values calculated by using the nonlinear fitting, as previously described [58].

Figures Captions

Fig 1. Textural characteristics of ABc-600 activated carbon. A- N_2 isotherm. B- DFT pore size distribution.

Fig 2. Thermogravimetric analysis of ABc-600 activated carbon.

Fig 3. FTIR spectra of ABc-600 activated carbon.

Fig 4. Kinetics of adsorption of captopril. A- 450.0 mg L^{-1}; B- 900.0 mg L^{-1} of captopril. Temperature 25°C, adsorbent dosage 1.5 $g.L^{-1}$, pH 7.

Fig 5. Isotherm of adsorption of captopril at 45°C, adsorbent dosage 1.5 g L^{-1}, pH 7, time of contact of 30 min between ABc-600 activated carbon and captopril solutions.

Fig 6. Nonlinear fitting of van´t Hoff equation for calculation of the thermodynamic parameters of adsorption.

Fig 7. Schematic diagram of the mechanism of adsorption of captopril onto ABc-600 activated carbon.

Fig 8. UV-Vis spectra of synthetic effluents before and after adsorption. A- Effluent A; B- Effluent B. Adsorbent dosage 1.5 $g.L^{-1}$, time of contact 1 h, temperature 25°C. For chemical compositions of wastewaters, see Table 1.

List of Figures

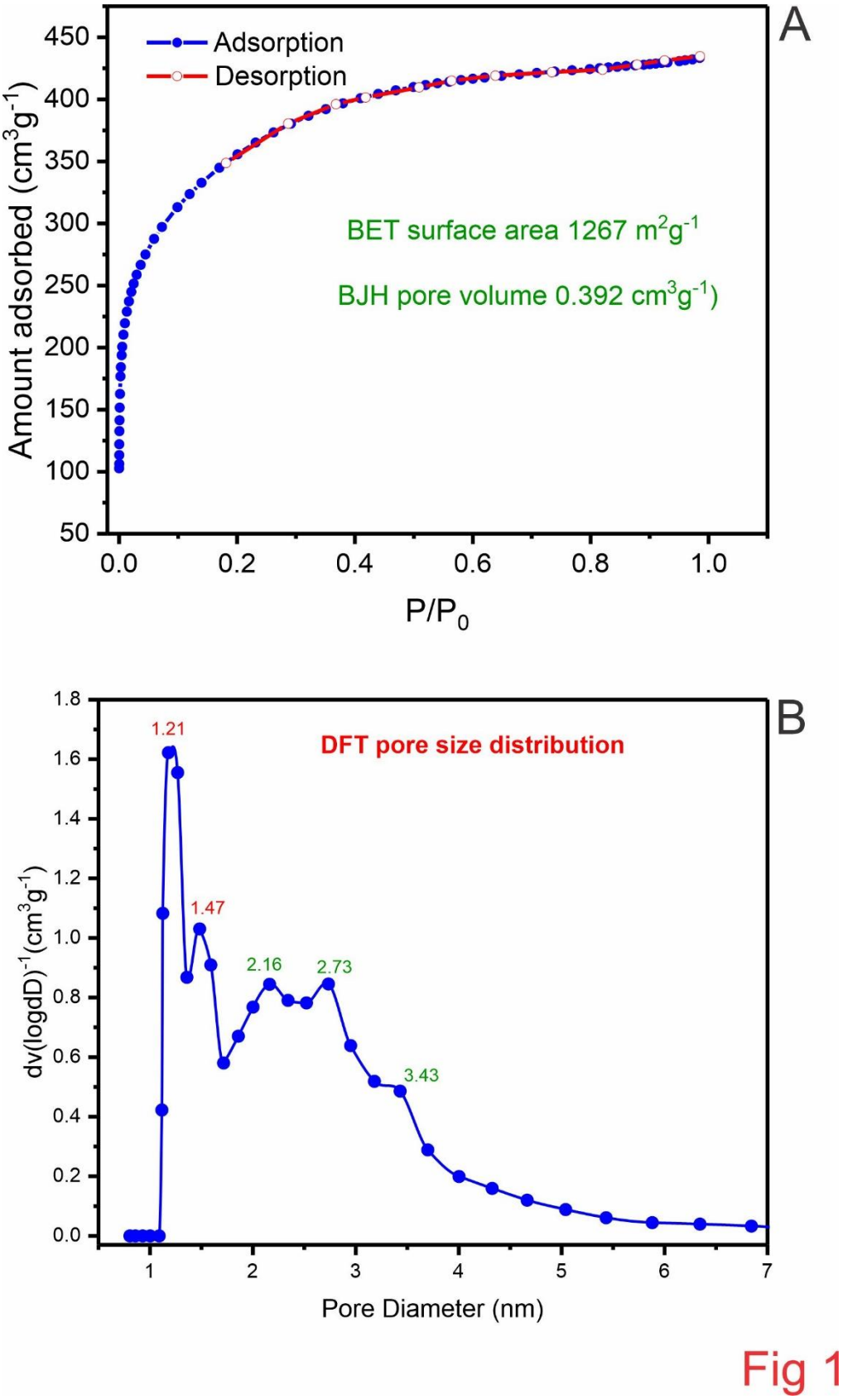

Fig 1

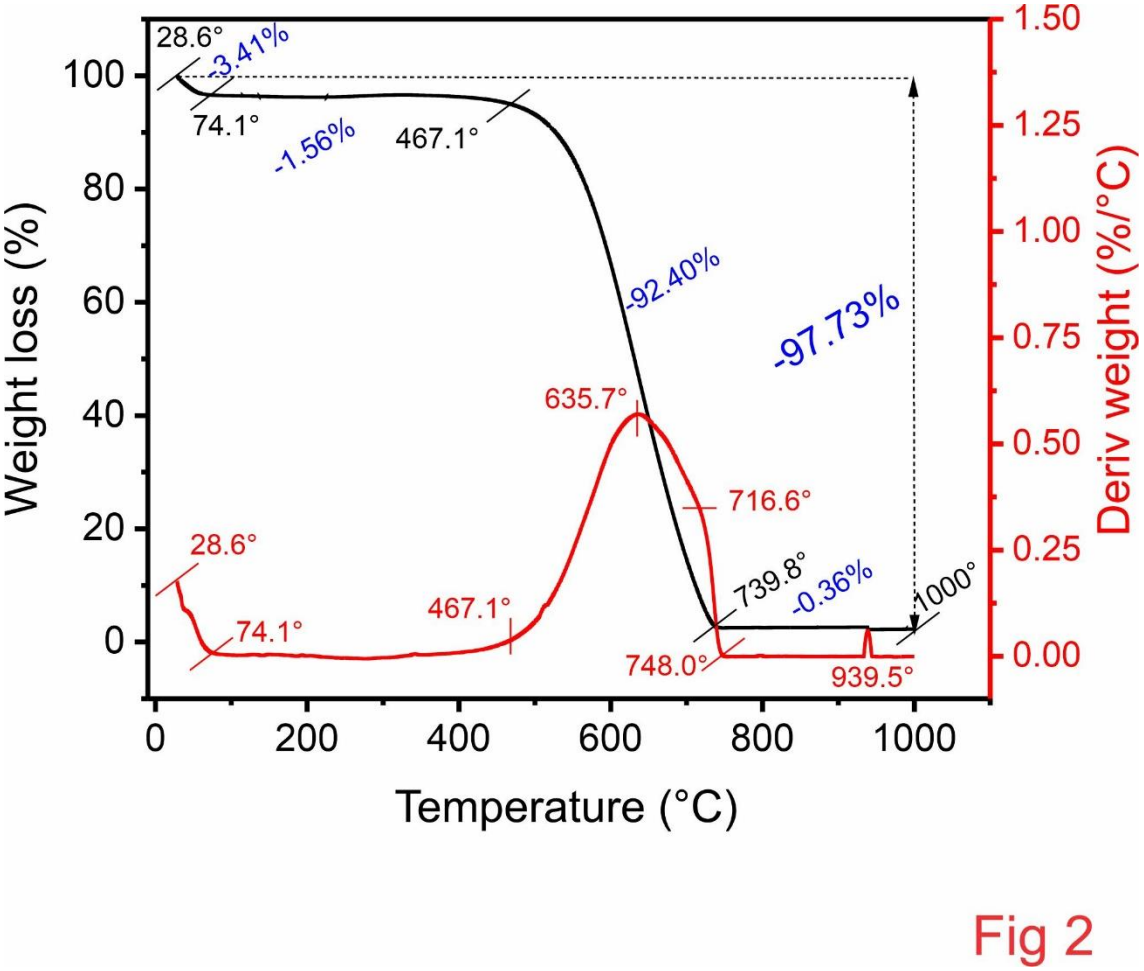
28.6°
-3.41%
74.1°
-1.56%
467.1°
-92.40%
-97.73%
635.7°
716.6°
739.8°
-0.36%
1000°
748.0°
939.5°
28.6°
74.1°
467.1°
Weight loss (%)
Deriv weight (%/°C)
Temperature (°C)
0
20
40
60
80
100
0.00
0.25
0.50
0.75
1.00
1.25
1.50
0
200
400
600
800
1000

Fig 2

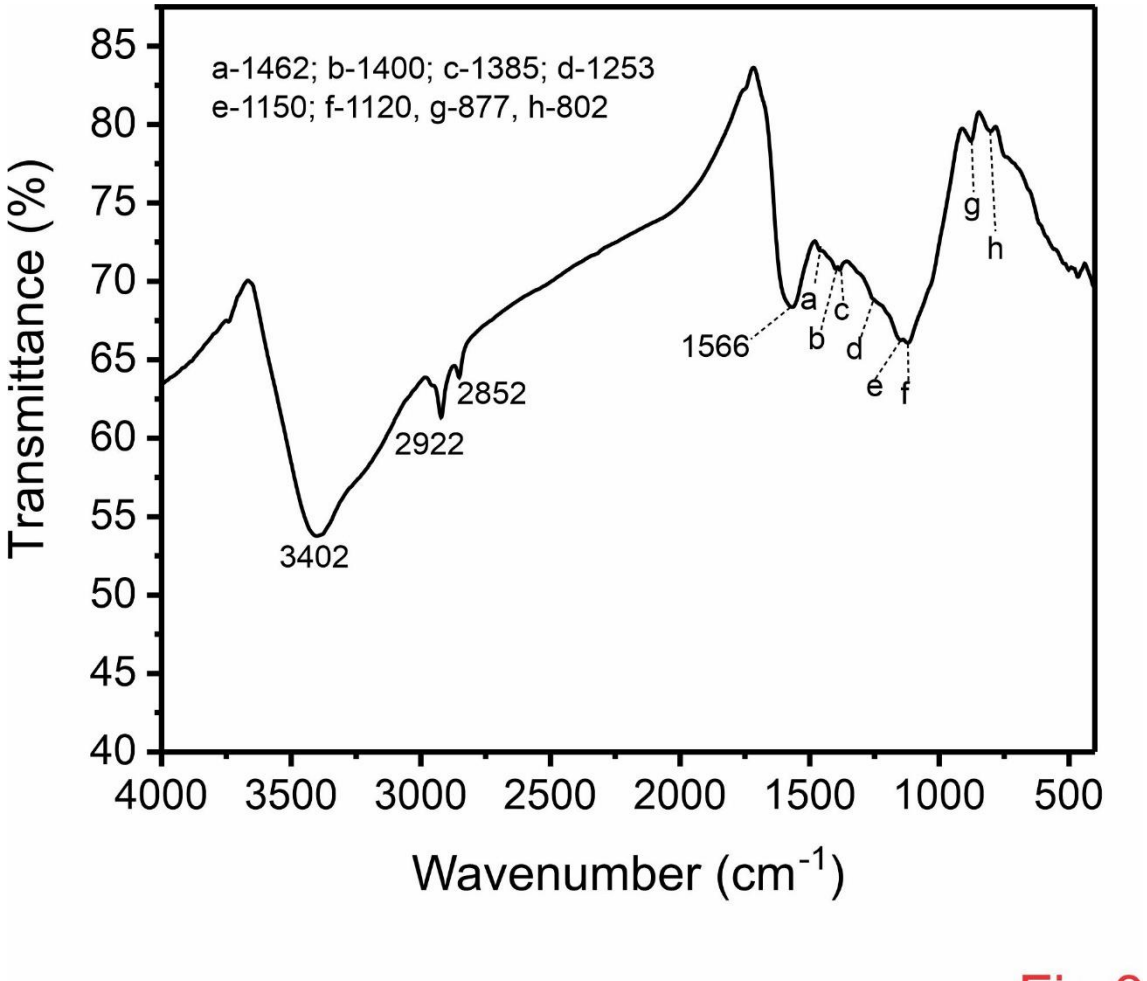
a-1462; b-1400; c-1385; d-1253
e-1150; f-1120, g-877, h-802
Transmittance (%)
Wavenumber (cm-1)
3402
2922
2852
1566
a
b
c
d
e
f
g
h

Fig 3

785

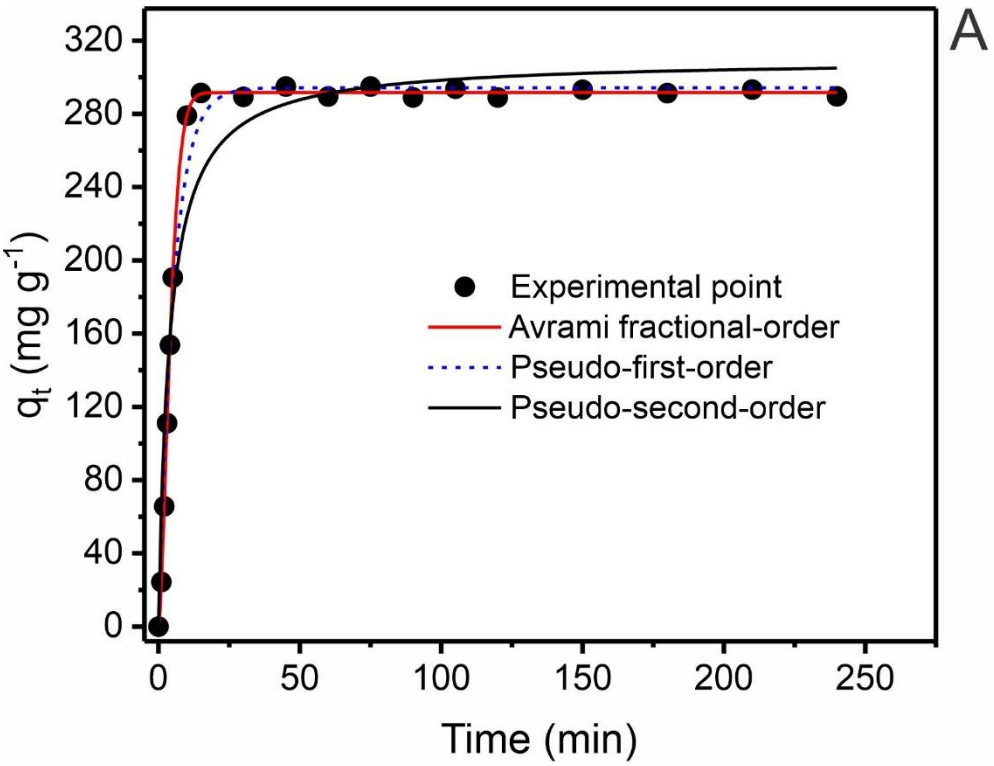

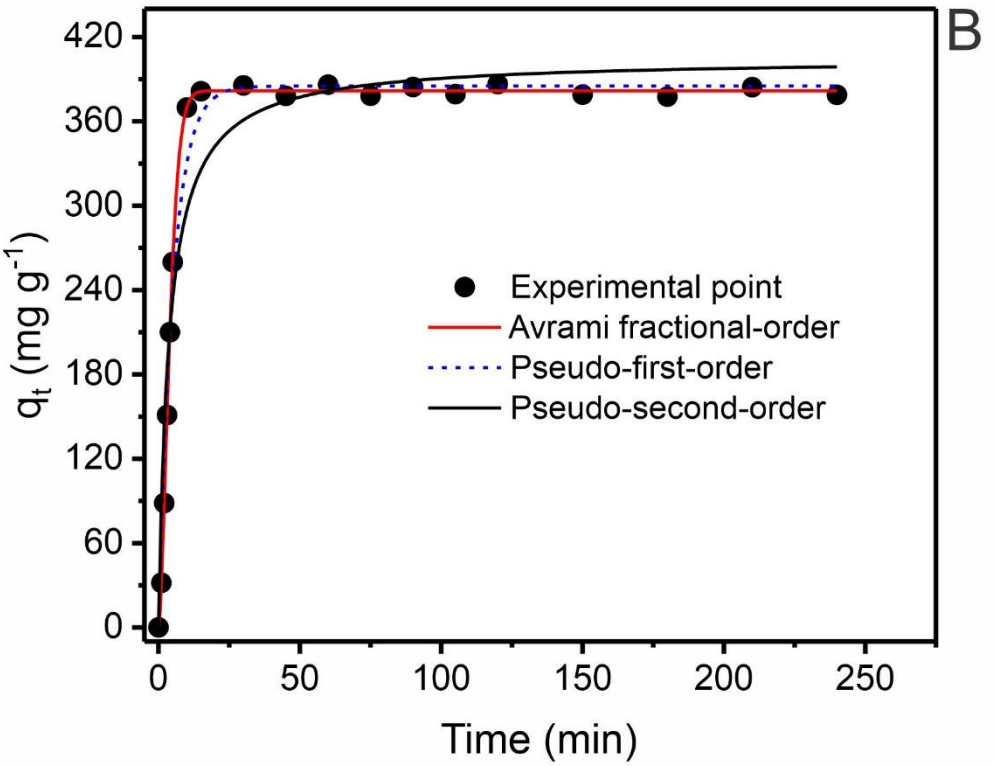

Fig 4

786

787

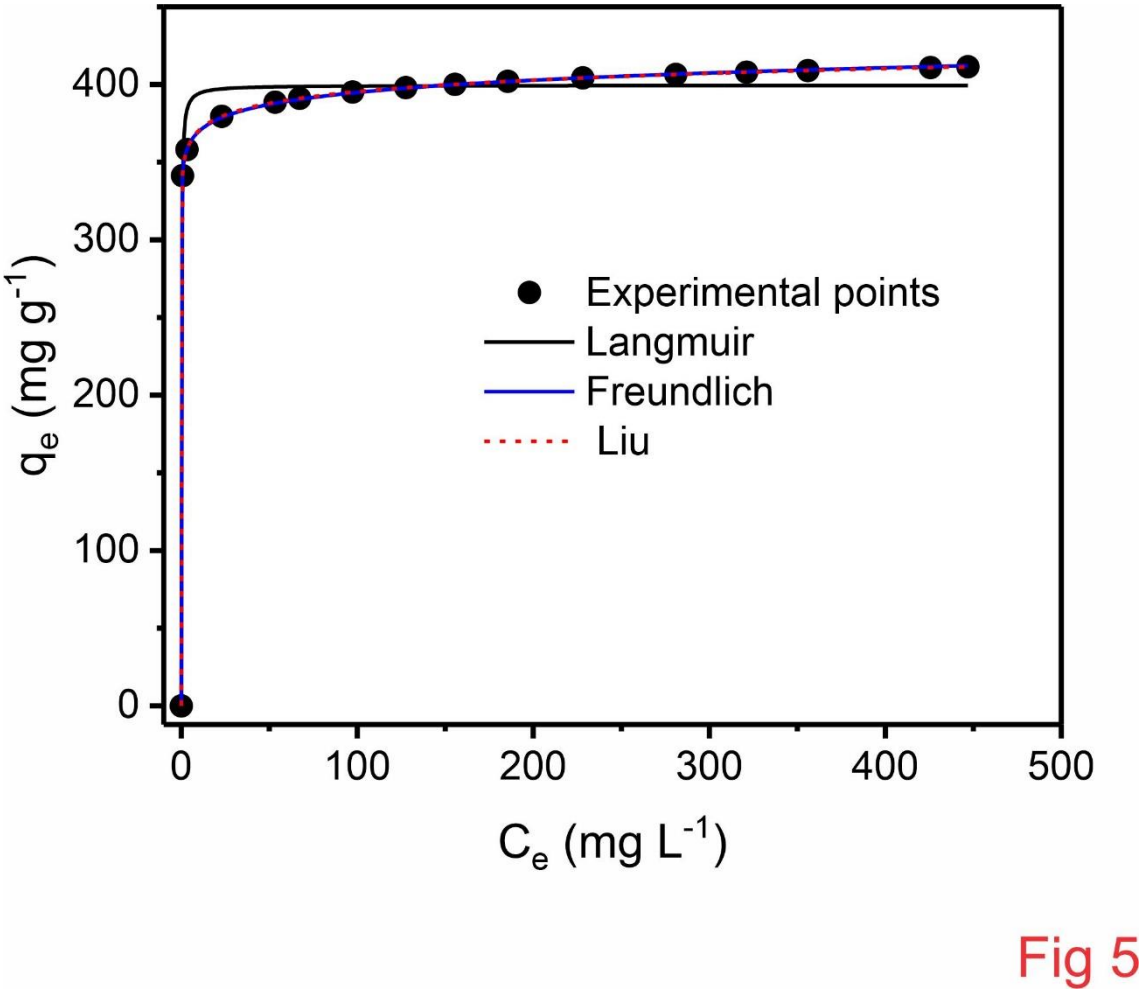
400
300
200
100
0
q_e (mg g^{-1})
0
100
200
300
400
500
C_e (mg L^{-1})
Experimental points
Langmuir
Freundlich
Liu

Fig 5

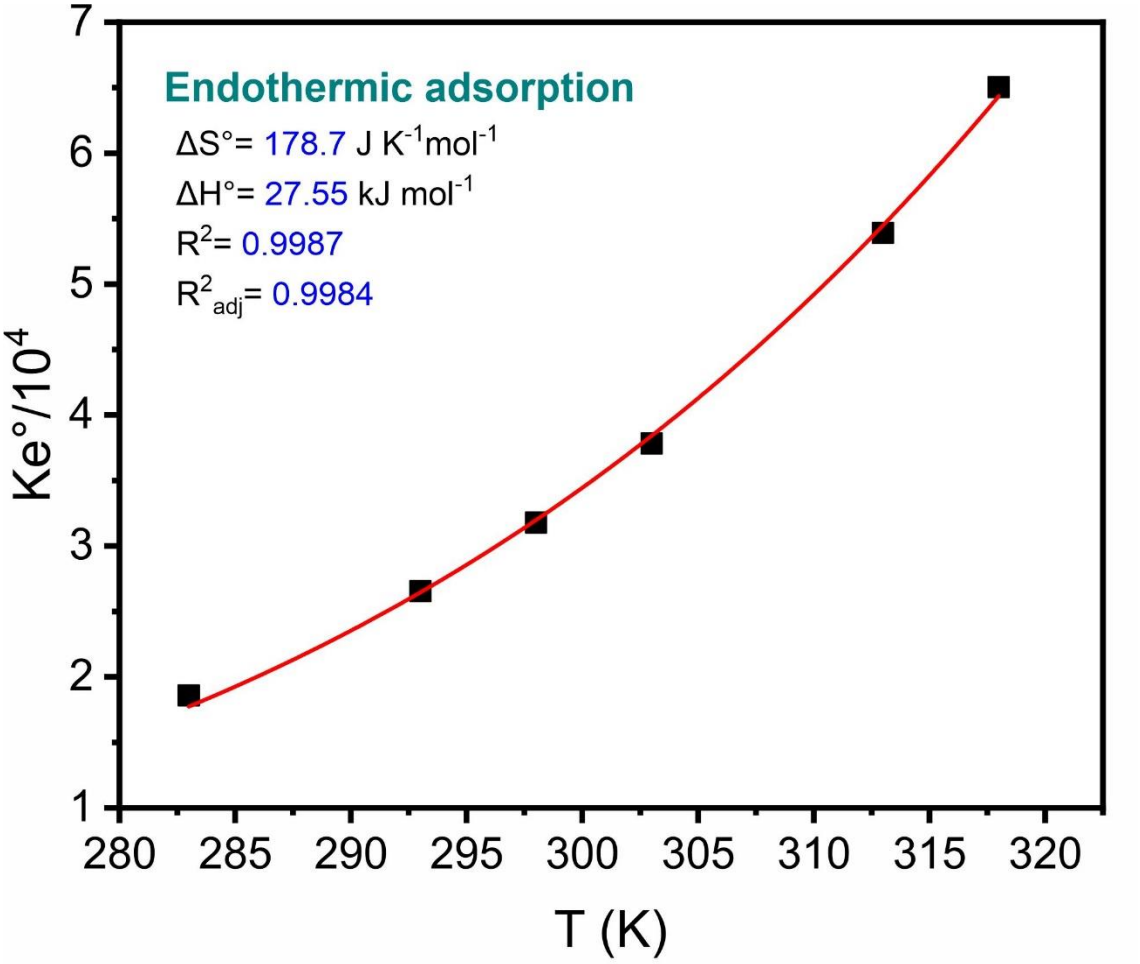
Endothermic adsorption
ΔS°= 178.7 J K-1mol-1
ΔH°= 27.55 kJ mol-1
R2= 0.9987
R2adj= 0.9984
Ke°/10^4
T (K)
1
2
3
4
5
6
7
280
285
290
295
300
305
310
315
320

Fig 6

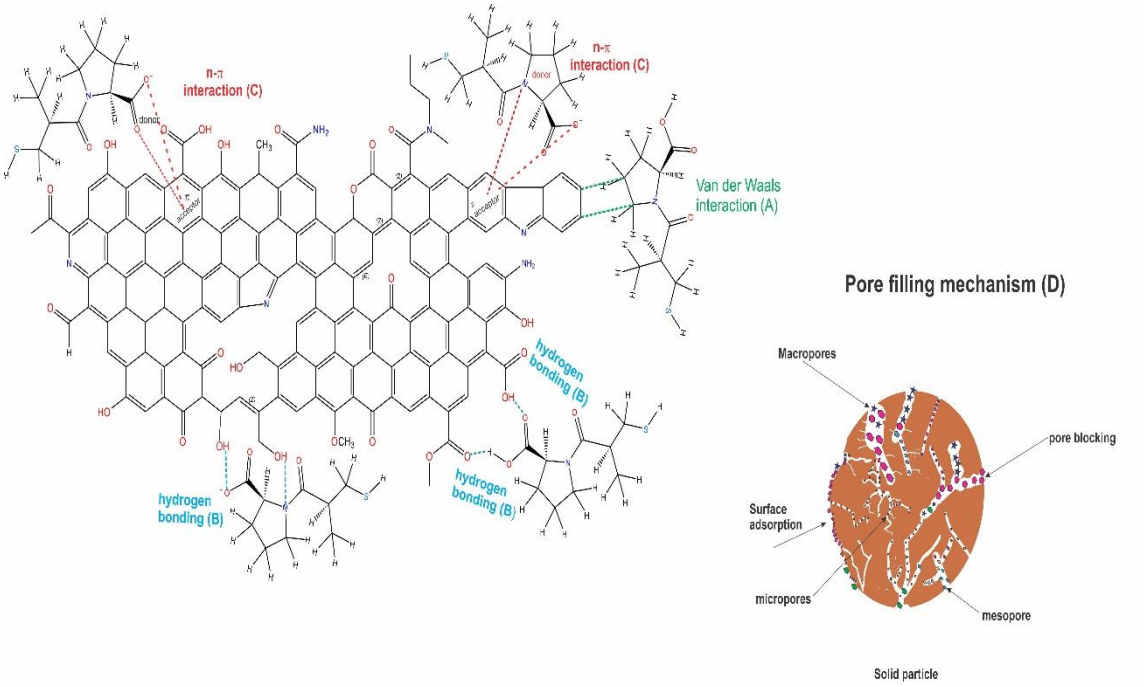
π-π interaction (C)
π-π interaction (C)
Van der Waals interaction (A)
hydrogen bonding (B)
hydrogen bonding (B)
hydrogen bonding (B)
Pore filling mechanism (D)
Macropores
pore blocking
Surface adsorption
micropores
mesopore
Solid particle

Fig 7

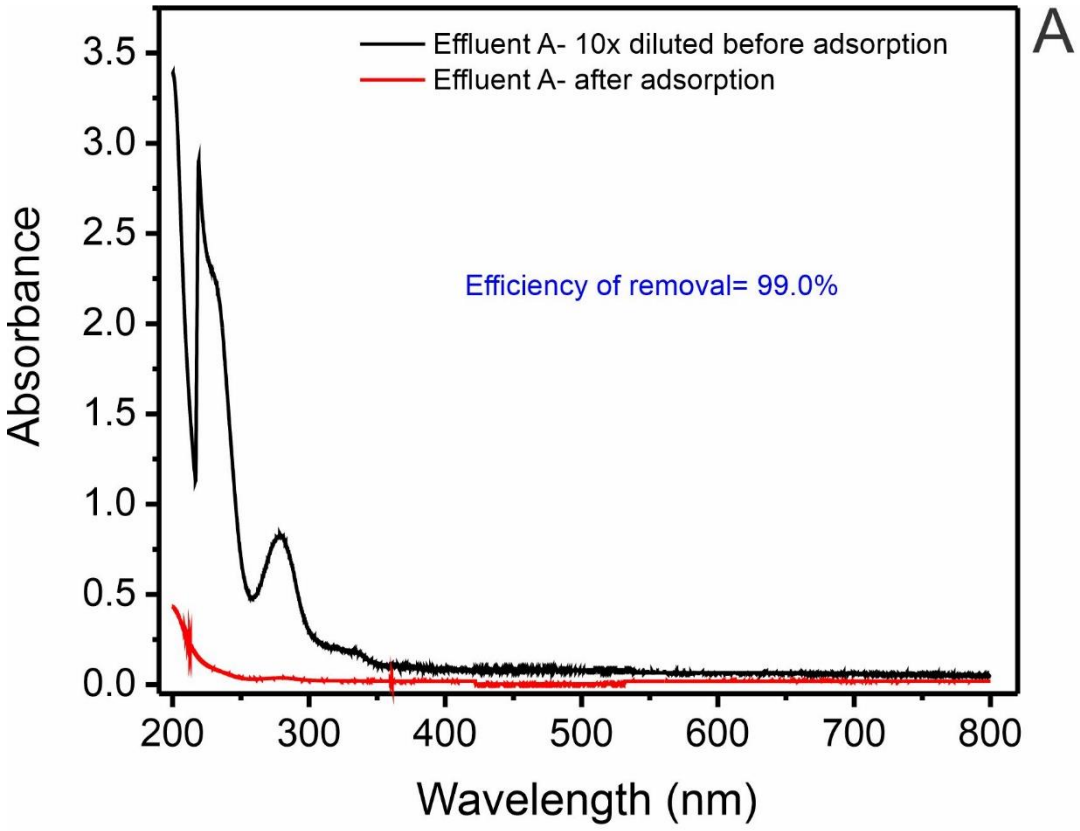
A
Effluent A- 10x diluted before adsorption
Effluent A- after adsorption
Efficiency of removal= 99.0%
Absorbance
Wavelength (nm)
0.0
0.5
1.0
1.5
2.0
2.5
3.0
3.5
200
300
400
500
600
700
800

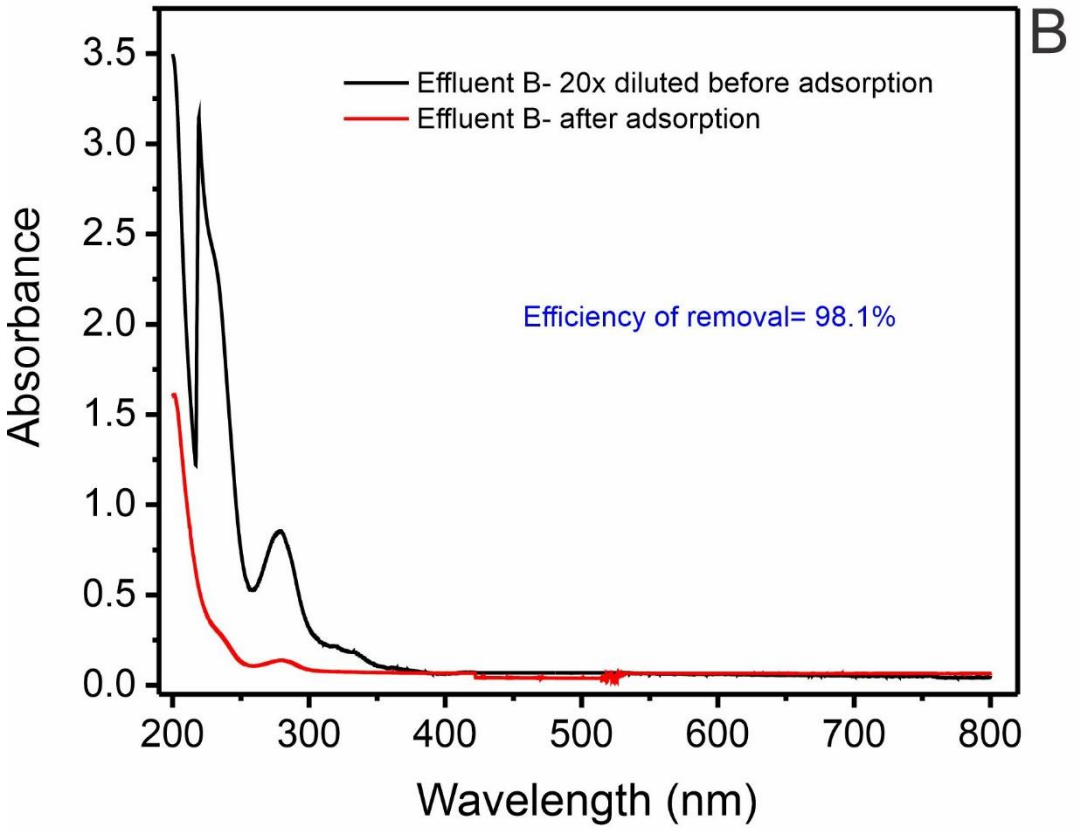
B
Effluent B- 20x diluted before adsorption
Effluent B- after adsorption
Efficiency of removal= 98.1%
Absorbance
Wavelength (nm)
0.0
0.5
1.0
1.5
2.0
2.5
3.0
3.5
200
300
400
500
600
700
800

Fig 8

817